Preprint submitted to Elsevier
A rigged model of the breast for preoperative surgical planning

Arnaud Mazier[1], Sophie Ribes[2], Romain Testylier[2], Frédéric Van Meer[2], Benjamin Gilles[2], François Faure[2] and Stéphane P.A. Bordas[*1,3]

[1]Department of Computational Science, Université du Luxembourg, Esch-sur-Alzette, Luxembourg
[2]Anatoscope, Montpellier, France
[3]China Medical University Hospital, China Medical University, Taichung, Taiwan

May 3, 2021

Keywords: Surgical planning, Model-based registration, Animation, Anatomical variability, Breast
Word Count: 3500

[*]Corresponding author: Department of Computational Science, Université du Luxembourg, Esch-sur-Alzette, 2, avenue de l'Université, Luxembourg / Telephone: +352 621 131 048 / Fax: +352 46 66 44 35567 / Email: stephane.bordas@me.com

Abstract

In breast surgical practice, various scans and medical examinations are performed before surgery. This includes identifying landmarks defining the operating procedure. In most cases, the position of the patient during the scan is vastly different from the one encountered during the operation. We address the challenge of mapping preoperative information to the operating field, with the following constraints: registration has to be done in less than 10 seconds to be compatible with a clinical workflow; the cost of the device must be small and we assume data scarcity, i.e. that our database has twenty scans of patients at most. We build anatomical complexity through a skinning model comprised of scalable bones (to account for pose and morphological variations) and deformable organs (blendshapes, to account for anatomical variations). Similar to animation rigs used in computer graphics, and in contrast to statistical approaches, we manually design a model with some desirable properties, using a reduced number of well-chosen degrees of freedom. Meaningful constraints can be applied to the registration depending on the context, and the trade-off between precision and complexity can be optimized. The result is a surface mesh of the patient obtained in less than 1 minute (scan and reconstruction included) and a registration method that converges within a few seconds (3 maximum), reaching a mean absolute squared error of 2.3 mm for mesh registration and 8.0 mm for anatomical landmarks. The registered model is used to transfer surgical reference patterns on any patient in any position.

1 Introduction

In 2018, breast cancer was the second most prevalent cancer with more than 2 million cases and its incidence rate increased by 0.3% per year [8]. Surgery remains one of the most common treatments, in 2016, nearly one-half of patients with early-stage (stage I or II) breast cancer underwent breast-conserving surgery [8]. The least invasive and traumatic operation, lumpectomy, consists of removing the breast tumor including surrounding tissues. Before surgery, the surgeon draws surgical patterns on the patient in a preoperative position (standing) and then, surgery is instantly done in the intra-operative stance (supine). These patterns, also called surgical drawings are part of the preoperative planning procedure; they can be important anatomical landmarks or a visual map that will guide the tools of the surgeon [24] [25]. The success of the operation is highly dependent on the said preoperative planning and will influence the final breast shape [27]. However, surgical drawings require experience and accuracy that can be challenging for young surgeons.

As the surgeon usually spends less than one minute on the drawing, timing is critical and imaging should be rapid to be compatible with the

clinical timing [5]. 3D surface imaging has proven to be a helpful technology in preoperative planning, especially for estimating breast parameters such as volume, shape, and symmetry [7]. These imaging techniques are fast and accurate but are still not widely used mainly due to the high cost of the devices [31].

Patient-specific models can be obtained in many manners. One of the most popular methods is to create a well-known model and deform it to fit the patient's data, namely registration. For example, [19] [18] directly reconstruct the breasts of patients with a low-cost depth camera coupled with non-rigid registration.

Other methods like free form deformation algorithms can deform an object by warping the whole space in which the object is embedded instead of warping the object directly. For example, [3] coupled rigid registration to free form deformation algorithms to register the breast from one position to another one.

The finite element method also uses surface scan registration to estimate unknown material parameters by minimizing the distance between the simulations results and the patient's data [9]. To reduce fitting error, all previous registration methods use a high number of degrees of freedom which leads to computational costs that are incompatible with surgical practice.

Statistical models also tackle this problem by using 3D morphable models. These statistical shape models are obtained by using dimensionality-reduction methods like Principal Component Analysis (PCA) to a set of training shapes. [29] and [17] combined 3D morphable models with additional landmarks to impose breast shapes constraints for improving the fitting of the model. These robust methods are faster than non-rigid registration but rely on a large database ($3.15s$ per scan on average with a database of 310 scans in [29])

Therefore, in all previous models, all patients had a quasi-similar posture. Indeed, non-linear transformations such as large articulated movements can be hard to model. In our patient database, we noticed a non-negligible pose variation that makes all previous methods difficult to apply. Learned-models overcome this issue by proposing neural networks that reproduce nonlinear mesh deformation effects as a function of pose information. These methods are widely used for their robustness, flexibility, and efficiency [6] [4]. Hence, the size of the training set required to account for pose and morphological variations across the population can be large and difficult to collect.

In this context, inspired by computer graphics, we propose to mix modes. We used a linear anatomical surface space of deformation to account for morphological variations known as blendshapes [21]. These deformers can be combined with a virtual skeletal connected to the surface of the model to consider pose variations, namely skinning [14].

In terms of model flexibility, the closest work is the SMPL (Skinned Multi-Person Linear Model) [22]. The main concept of SMPL is the use of

corrective human body-shape and pose-dependent shape variation, learned from thousands of 3D body scans, to improve the accuracy of the skinned model. Originally designed for graphics purposes, the learned-model has been extended to the medical field. For example, [12] fit its SMIL to RGB-D sequences of freely moving infants for early detection of neurodevelopmental disorders. SMPL fulfills our timing and accuracy criteria. The main drawback of the model is the learning database, partially made of women wearing bras, which makes impossible to capture anatomical details that are only visible on naked-breasts. At the time of writing this paper and to our knowledge, no open-source database of 3D scans of exposed chest is available.

In this paper, we propose a flexible model that can fit a set of patients in different surgical positions, without any previous training phase. To ensure a quasi-instantaneous patient fitting, we developed a simple articulated model made of virtual bones to allow pose modifications. This model is made more adaptive by allowing the scalability of these bones to cater for variations in body morphologies. Moreover, we used a simple linear model of body shapes to account for physiological variations in breast shape. In the end, our model fits a scan in less than 3 seconds, is robust to noise, incomplete data, posture, and morphological variations of patients.

2 Method

2.1 Data acquisition

To obtain a 3D surface mesh of the patient, we used a depth camera[1]. This scanning device suffers from a high noise-sensitivity and the possible creation of spurious gaps within the mesh. However, it satisfies our criteria in terms of rapid acquisition time, user-friendly interface, and reasonable price.

The acquisition was made on 7 women, in preoperative and intra-operative positions. Their age varies between 30 and 70 years and their breast size from 95A to 110C with one notable case of asymmetry. All the patients were diagnosed with breast cancer and chose lumpectomy as the most suitable treatment, under medical recommendation. After obtained consent from the 7 patients for the study, scans were performed by the surgeon without any previous training. The result is a surface mesh of the patient obtained in less than 1 minute, scan and reconstruction included.

2.2 Rigging

Skeletal animation or rigging is a technique in computer graphics to animate an articulated object. The "rig" is usually a hierarchical set of interconnected parts called "bones". These bones are purely fictive and connected through joints designed to mimic as best as possible the motion of a human. Usually,

[1] Structure Sensor by Occipital: https://structure.io/

the rig is done manually as it depends on the animated surface shape. Nowadays, much 3D software offers this feature, but rigging requires experience and skills to know the number and position of the bones. Previous work has been done to automatically generate the skeleton based on the 3D surface mesh [1].

Each bone will be considered as a rigid-scalable object, meaning that each bone will have 9 absolute DOFs (3 rotations, 3 translations, and 3 for the scale). The relative motion of the bones will be constrained by the joints. We compute local rotations and translations of the joints by computing relative transformations at a rigid point attached to the scalable bones, represented by the spheres in figure 2a. Then, constraints are applied through Lagrange multipliers on local rotations and translations [30]. Quaternions are used to define the axis angle of every bone. From them, we compute a local rotation matrix.

2.3 Skinning

Skinning is the next step to animate the articulated model. It consists of deforming the surface mesh (i.e the skin of the model) depending on the pose of the rig [14] [13] [20]. This can be achieved through blend weights that adjust the influence of each skeletal bone on the skin. In figure 2b, we displayed the colormap of the blend weights associated with the lower bone. The red regions are rigidly attached to the bone and follow the bone's motion, conversely, blue areas are not affected by the movements of the bone. The blend weight matrix can be manually given by the user or can be automatically calculated by 3D modeling software such as Blender [2].

In a simple case on the figure 1a, we designed 2 bones linked by a spherical joint and applied a simple 45 degrees rotation around the z-axis on the upper bone. Each bone is connected to the cuboid through a blend weight matrix. We observe a bending of the structure caused by the rotation of the bone, only the upper part of the object is deformed because the surface is mainly affected by the upper bone via the blend weight matrix.

In this study, the model is more complex with $K = 9$ bones and $N = 2200$ vertices as shown in figure 2a. We use the following notations: $R_j(q)$ the rotation matrix of the j^{th} bone obtained from the quaternion rotation, T_j the associated vector bone offset and S_j the scale matrix with a scale coefficient for each direction. As a result, with a given set of K bones, bones rotation $R(q) = [R_1(q), ..., R_K(q)]$, bone offset $T = [T_1, ..., T_K]$, bone scale $S = [S_1, ..., S_K]$. By calling the elements of the blend weight matrix $w_{j,i}$ ($w \in \mathbb{R}^{K \times N}$) and the rest template mesh vertices v_i ($v \in \mathbb{R}^{N \times 1}$). The computed vertices M_i are given by the equation of the Linear Blend Skinning (LBS):

[2] https://www.blender.org/

$$M_i(R(q), S, T) = \sum_{j}^{K} w_{j,i}(R_j(q)S_j v_i^T + T_j), \tag{1}$$

2.4 Blendshapes

Originally from computer graphics, [26] used blendshapes for the first time in facial animation. Years later, blendshapes are implemented in all animation software for providing realistic and quick facial expressions to animated characters [15] [21]. Now widely used for efficient geometrical deformation [23], blendshapes are deformed versions of a template mesh. For our model, an artist created $A = 55$ blendshapes affecting global features such as shoulders or belly size as well as more local ones such as nipples and aureole shapes. Let v denotes the vertex positions of the template mesh, B the blendshape function computing the deformed vertex positions and b_k the k^{th} shape displacement matrix, with $v, B, b_k \in \mathbb{R}^{N\times 3}$. Blendshape displacements provide a set of basis vectors that define a linear space which is used to generate a vector space, onto which the patient's shape is projected.

$$B(\alpha_k) = v + \sum_{k}^{A} \alpha_k b_k, \tag{2}$$

where A is the number of blendshapes and $\alpha_k \in \mathbb{R}^A$ the linear blendshape weights affected to each k^{th} blendshape. To ensure convexity and invariance for rotation and translation, these weights should fulfil the following conditions: $\sum_{i=1}^{n} \alpha_k = 1$ and $\alpha_k > 0, \forall k \in [\![1, n]\!]$. These 55 blending weights (α_k) can be used as degrees of freedom (DOFs) for our deformable model, we call α the vector storing the α_k values.

By combining different body shapes, the model can cover a large deformation space to fit several morphologies (figure figure 3) and can be easily enriched by adding more blendshapes. Blendshapes and Principal Component Analysis (PCA) are two possible linear models to create an anatomical space of deformation. Blendshapes are generally hand-crafted by an artist, whereas PCA modes are extracted from example data. As a result, blendshapes, contrary to PCA modes, do not make up an orthogonal basis (real inner product space), but are, in general, still independent. Besides, the modes generated by PCA, produced by linear operations are often difficult to interpret physically. The major drawback of blendshapes is the degeneration of the solution when the deformation involves large rotations [23]; which can be avoided with skinning methods.

2.5 Final model

In the final model, we combine the effect of blendshapes mixed with the scalable bones of the skinning. While blendshapes and scalable bones permit morphological variations between patients, rigging take care of adjustments in the patient's pose. The skin deformation due to pose variations is approximated by skinning, more precisely the blend weights imposed by the artist. By injecting equation 2 into 1, we obtain:

$$M_i(R(q), S, \alpha, T) = \sum_j^K w_{j,i}(R_j(q)S_jB_i^T(\alpha) + T_j), \tag{3}$$

To avoid distortion of the model and to regularize the energy minimization we define 3 additional energy terms. A scale energy E_S to penalize the scale matrix of each bone towards its original scale (with $\mathbb{I}_3$ the order 3 identity matrix). A blendshape energy E_{BS} to regularize the blendshape weights towards 0 and a joint energy E_J to regularize the translations and the relative rotations of each joint to their initial configurations, respectively T_j^* and $R_j(q^*)$ for the j^{th} bone. With $\| \bullet \|$ the Euclidean norm, we obtain the following equations:

$$E_S(S) = \sum_j^K \| S_j - \mathbb{I}_3 \|^2, \tag{4}$$

$$E_{BS}(\alpha) = \| \alpha \|, \tag{5}$$

$$E_J(R(q), T) = \sum_j^K \| \log(R_j(q^*)R_j^{-1}(q)) \|^2 + \| T_j - T_j^* \|^2 . \tag{6}$$

2.6 Registration

To fit the skin of the model to the scan of the patient, we have chosen to minimize closest-point distances such as in the ICP algorithm [2]. More exactly, we used an octree structure to find the closest vertex on the scan from source vertices. Then, we projected the source point onto the closest primitive (triangle, edge, or point) around each closest vertex. It allows a more accurate registration than using point-to-point distances and differentiating 7 with respect to M_i can be easily done by computing the normals on the scan. The scanning process depends on the surgeon, some scans can be incomplete containing only the front view and artifacts, as shown in figure 9a. To improve the robustness of the algorithm against noise and local solutions, filters to reject outliers have been added (distance and normal threshold).

Based on correspondences established at each iteration, we identify the best set of parameters that minimizes the distance from the scan to the

deformed model. We define a data energy term that penalizes the squared Euclidean distance between the model vertices M_i and the target mesh V according to the closest point algorithm:

$$E_D(R(q), S, \alpha, T) = \sum_{(i,j)}^{N_{CP}} \parallel M_i(R(q), S, \alpha, T) - V_j \parallel^2, \tag{7}$$

where N_{CP} represents the index pairs found by the closest point algorithm and V_j is the closest point from M_i on the set of target mesh triangles. The total energy to minimize is :

$$E_{tot}(R(q), S, \alpha, T) = \frac{1}{\lambda_D} E_D + \frac{1}{\lambda_S} E_S + \frac{1}{\lambda_{BS}} E_{BS} + \frac{1}{\lambda_J} E_J \tag{8}$$

with $\lambda_D = 10e^{-3}, \lambda_S = 10e^{-2}, \lambda_{BS} = 10e^{-3}, \lambda_J = 10e^{-2}$ set empirically. We used a regularized Newton algorithm and stop the minimization when we reached our convergence threshold based on the distance compared to the last iteration.

As described in [30], we iteratively minimize equation 7 using an implicit integration of Newton's equation, using a compliant formulation to handle both stiff constraints (joint translations and rotations) and elastic terms in a stable manner. The solver finds a compromise between minimizing the distance to the data and the distortion of the reference model.

According to [10], we manually added 12 anatomical landmarks on the model (figure 9b) and on all scans in preoperative and intra-operative stance (respectively figure 9a and 9e). These landmarks were chosen for their easy reproducibility, as validation criterion for the registration and to possibly strengthen our registration. Indeed, without taking into account the landmarks in the registration, we achieve a mean absolute squared error (MASE) of 2.01 cm between the landmarks of the model and the scans, which is too large. Our registration approach offers the possibility to combine automatic vertex matching (closest-point algorithm) with manual vertex matching (landmarks). By enabling the surgeon to interactively select these landmarks, we can add a landmark energy term to penalize the squared distance between the landmarks of the model and the landmarks of the scans. The landmark energy E_L expression is similar to equation 7, but we replaced the closest-points index pairs by the corresponding landmarks index pairs.

$$E_{fin}(R(q), S, \alpha, T) = E_{tot} + \frac{1}{\lambda_L} E_L, \tag{9}$$

with $\lambda_L = 10e^{-4}$ also set empirically.

As shown in figure 4, by taking the landmarks into account in the registration, we reached a MASE of 8.03 mm on the landmarks without increasing our MASE on the mesh registration. This improvement is expected but highlights in some cases a bad matching of the closest point algorithm. Indeed

some landmarks such as nipples are geometrically significant on the mesh and can be detected by the automatic algorithm; others like the sternum are only textured information and are hard to be detected by the closest point. Manually adding the landmarks (takes less than 30 seconds) produces a more accurate registration for less computational time.

3 Result

We chose the Simulation Open Framework Architecture (SOFA [11]) to perform our registration onto 7 patients in preoperative and intra-operative stance.

In table 1, we computed for each scan the time needed to reach our stopping criterion as well as registration statistics of the surface and landmarks between the model and scan points. These results show that the registration is efficient and independent of the pose or the morphology. Assuming a good registration of the model on the scan, we can transfer a surgical pattern to the patient. To do so, we drew a given surgical pattern for breast lumpectomy (image 9b). As shown in image 9a and 9d, the surgeon draws 5 shapes, 2 delineating the upper and lower sternum, 2 for the right and left breast, and the last circle represents a projection of the tumor. As the tumor drawing is designed according to the patient-specific MRI, we are only focused on drawing the sternum shapes and delineating breasts. We had also superimposed the drawing of the surgeon (in black) and the drawing of the model (in white), respectively image 9c in preoperative and 9f in intra-operative stance.

Besides, we studied the effect of blendshape numbers on the performances of the model. As shown on figures 5 and 6, increasing the number of blendshapes reduces the MASE. Indeed, by expending the number of blendshape, the deformation space of the model is expended; as a result, the model can fit more complex body shapes. For the preoperative stance (figure 5), we observe that after 25 blendshapes we obtain a slight improvement of the solution. In the intra-operative stance (figure 6), we see that even with 55 blendshapes, the MASE is still decreasing, showing that the result can probably be improved by taking more blendshapes. Determining the right amount of blendshape can be delicate because one blendshape can be meaningful for one particular morphology but worthless for another one. For example, in figure 6, blendshape 44 has a significant impact on the majority of the patients but not for *Patiente 0* and *Patiente 6*. A compromise has to be found between accuracy and registration time. Indeed, by increasing the number of blendshapes, the number of DOFs is also increasing leading to higher registration time. For the proposed application, 55 blendshapes are a reasonable give-and-take with a mean accuracy lower than $3mm$ for the surface registration and an execution time inferior to $3s$.

Finally, we conducted a sensitivity analysis of the model's parameters in both configurations. As we empirically chose the values of $\lambda_D, \lambda_S, \lambda_{BS}, \lambda_J$ and λ_L, we investigated the impact of these parameters on the surface and landmarks MASE. To do so, we modified one particular parameter while fixing all other parameters to their original value and calculated the mean MASE for all patients. As mentioned in section 2.6, these parameters represent the impact of specific energies on the entire system (equation 9). The results are displayed in preoperative configuration, in figures 7 and 8, but the curves are similar in intra-operative stance. This study highlights the following points:

- Decreasing the value of λ_D is increasing the impact of E_D (equation 7) in the total energy and improve the surface MASE.
- Decreasing the value of λ_L is improving significantly the landmark MASE. Hence, decreasing λ_D for improving the surface MASE does not improve the landmark MASE, this highlights the bad matching of the closest-point algorithm.
- Other parameters do not have a strong impact on the MASEs but by increasing their values, both MASEs slightly decrease. Indeed, as $\lambda_S, \lambda_{BS}, \lambda_J$ prevent model distortion, reducing their values force the model to its initial configuration. Conversely, selecting a value upper than 10 leads to singularities on the model.

4 Discussion

In the present study, we registered a simplified breast-model on multiple patients in the preoperative and intra-operative configuration. We used a skinning model comprised of scalable bones and blendshapes to provide a trade-off between precision and time-efficiency. We showed that Linear Blend Skinning was a good approximation of the bone joints motion and allow the model to fit different poses. LBS can be subject to volume loss or "candy-wrap" effect when joints rotations are too important, this can be alleviated with Dual Quaternion Skinning [16] or Implicit Skinning [32]. So far, we did not observe such behaviors in our application. Moreover, morphological differences, as well as soft-tissue deformation induced by different poses, are challenging to model and were approximated by blendshapes. The robustness of the model was demonstrated through a sensitivity analysis showing that a balance has to be found between λ_D and λ_L enhancing respectively the accuracy of the mesh registration and the accuracy of the landmark registration. Finally, the model is flexible and can be easily modified by tuning the regularization parameters or by adding new blendshapes, landmarks, and bones.

We showed a concrete clinical application of breast patient-specific modeling for preoperative surgery drawing based on real data with the following results: on average, 2.35mm for the surface MASE, 8.03mm for the landmarks MASE, and 2.03s for the execution time. The results obtained in this study are congruent with those present in the literature. [29] used 3D Morphable Models of the breast to fit two possible inputs: 2D photos and 3D scans. For 310 3D scans, an average distance error of 2.36mm in 3.15s is obtained with a standard deviation of 0.18mm. While these results are similar in magnitude to those of the present study, [29] obtain a lower standard deviation error probably due to the high number of scans.

Our application is mainly focused on lumpectomy but the methodology is general and can be compatible with other surgical patterns such as mastectomy or mammary reduction. The method can even be generalized to other body parts but will require to create a new rig, mesh, and blendshapes. Our approach could be improved by automatically detecting the landmarks (using the scan's textures for instance). Those are for now identified manually by the surgeon which is an advantage for flexibility but a drawback for automation. To reduce the computational time, we also used a coarse mesh but refinement of the mesh can lead to better registration. Validation on a larger population for creating a statistical database would be a useful step forward. This could be done by adding a Bayesian regularisation term [28] to the energy minimization term. The registration provides a patient-specific mesh, ready for biomechanical simulations, and can be the base for pre to intra-operative mapping of tumors using the finite element method.[2]

Acknowledgements

This study was supported by European Union's Horizon 2020 research and innovation programme under grant agreement No 811099 and the Marie Sklodowska-Curie grant agreement No. 764644. The medical images used in the present study were obtained in Hopital Arnaud de Villeneuve, Département de Gynécologie Obstétrique in collaboration with Dr Gauthier Rathat.

Conflict of interest statement

The authors of this work have no conflicts of interest to disclose.

List of Tables

List of Figures

Table 1: Registration statistics errors for preoperative and intra-operative stance

Preoperative configuration

Patient	**Time** (s)	**Surface distance error**			**Landmarks distance error**			
		Mean (mm)	Std (mm)	Max (mm)	Mean (mm)	Std (mm)	Max (mm)	Min (mm)
0	1.98	2.31	3.24	23.7	8.24	3.42	13.8	3.74
1	2.17	2.22	4.06	45.6	8.70	4.99	16.2	4.68
2	2.11	2.58	2.94	35.9	11.03	5.88	25.0	2.34
3	1.32	2.23	2.15	14.5	8.98	3.97	16.2	1.61
4	1.38	2.43	2.88	25.0	8.17	6.54	20.7	0.94
5	2.23	2.23	3.39	23.3	7.22	3.46	11.9	1.21
6	1.79	2.87	3.71	51.5	6.89	5.72	22.9	3.53
Mean	**1.85**	**2.41**	**3.19**	**31.4**	**8.46**	**4.85**	**18.1**	**1.98**

Intra-operative configuration

Patient	**Time** (s)	**Surface distance error**			**Landmarks distance error**			
		Mean (mm)	Std (mm)	Max (mm)	Mean (mm)	Std (mm)	Max (mm)	Min (mm)
0	2.01	2.39	3.48	31.9	9.36	3.68	14.9	3.40
1	1.90	2.11	3.00	17.7	7.96	4.13	15.2	1.54
2	1.99	2.14	3.13	20.1	7.23	3.74	14.0	1.02
3	2.54	2.33	2.78	19.6	3.95	3.40	12.3	0.37
4	2.14	1.85	2.78	24.3	7.32	3.44	11.2	0.21
5	3.01	2.44	2.86	20.4	7.03	4.91	15.8	2.84
6	1.80	2.70	3.43	30.6	10.39	4.36	19.6	2.85
Mean	**2.20**	**2.28**	**3.06**	**23.5**	**7.61**	**3.95**	**14.7**	**1.75**

(a) (b)

Figure 1

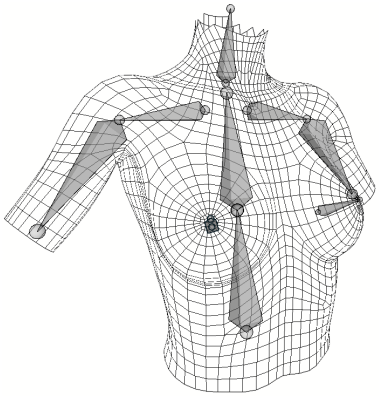

(a)

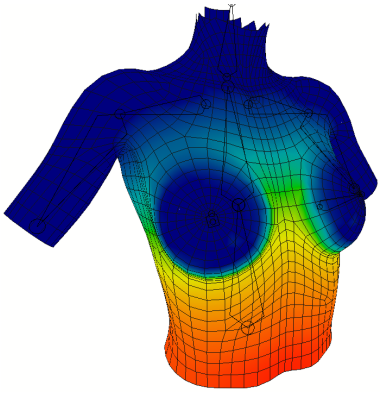

(b)

Figure 2

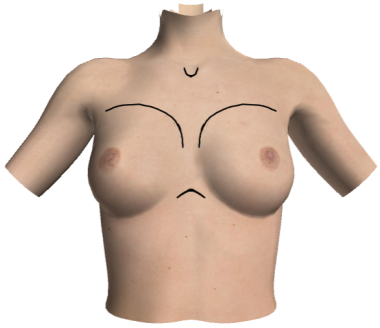

(a)

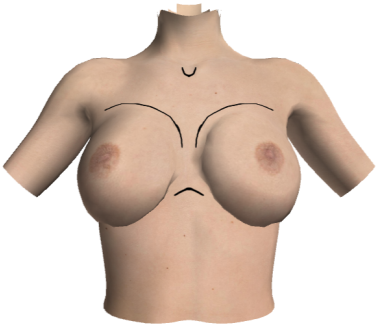

(b)

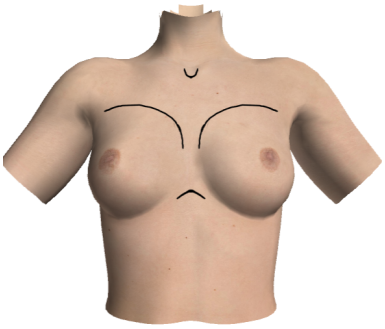

(c)

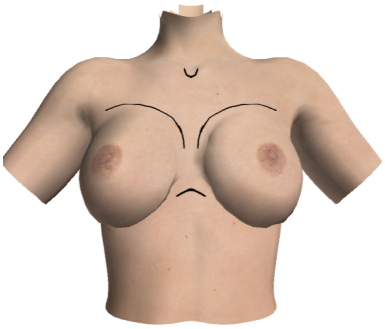

(d)

Figure 3

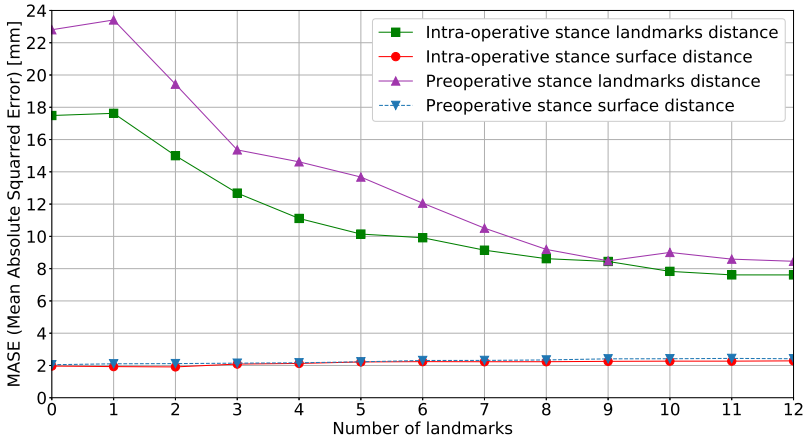

Figure 4

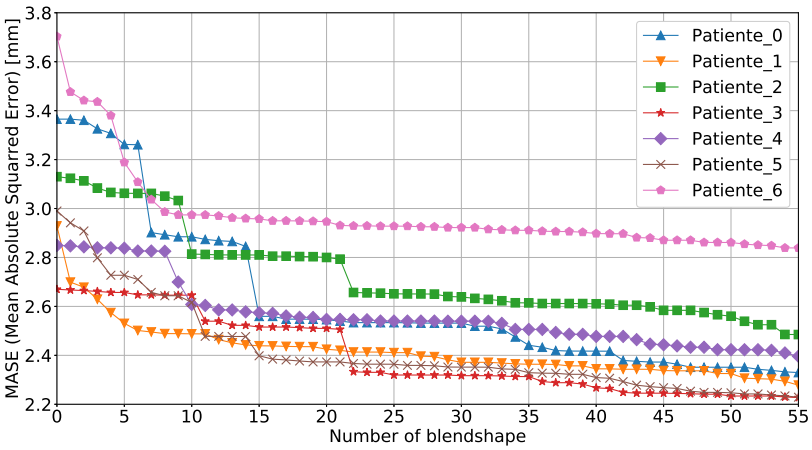

Figure 5

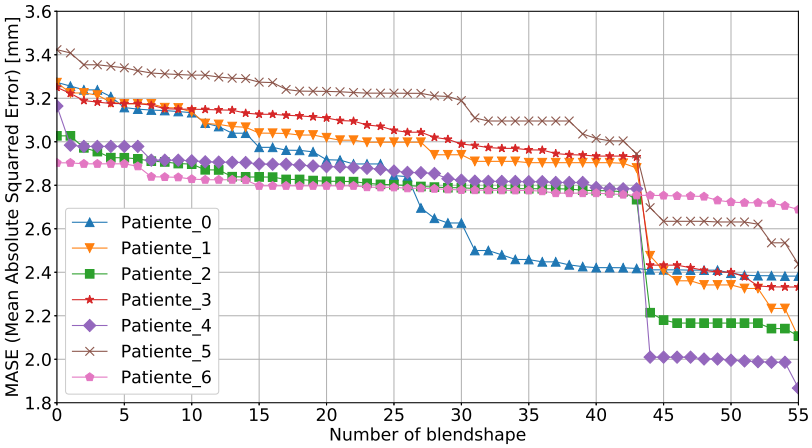

Figure 6

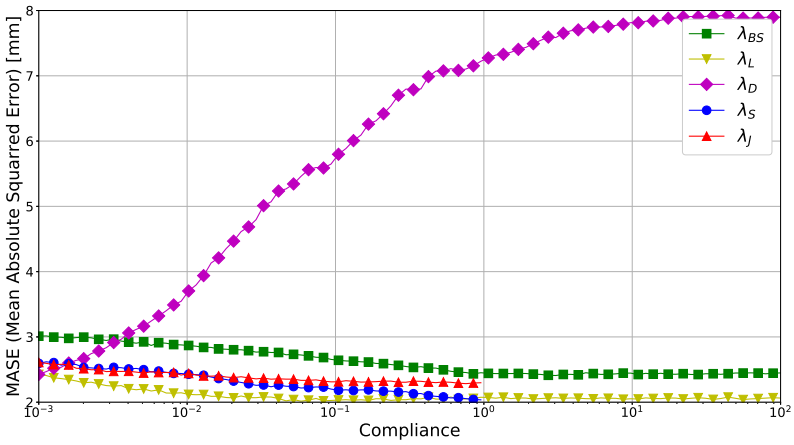

Figure 7

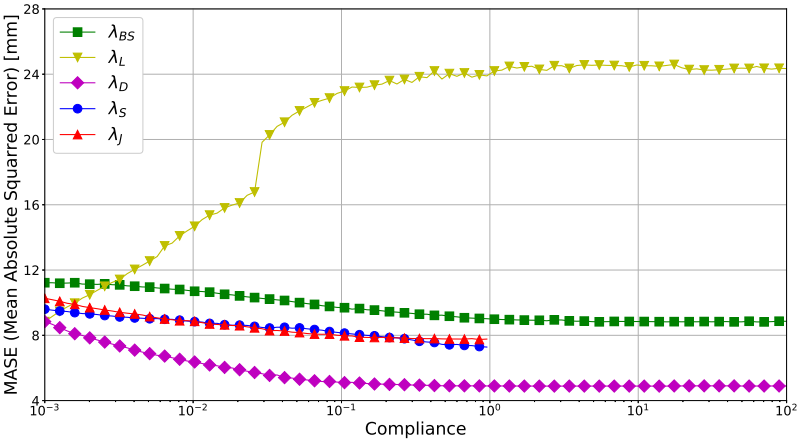
λ_{BS}
λ_L
λ_D
λ_S
λ_J
MASE (Mean Absolute Squarred Error) [mm]
Compliance
28
24
20
16
12
8
4
10^{-3}
10^{-2}
10^{-1}
10^{0}
10^{1}
10^{2}

Figure 8

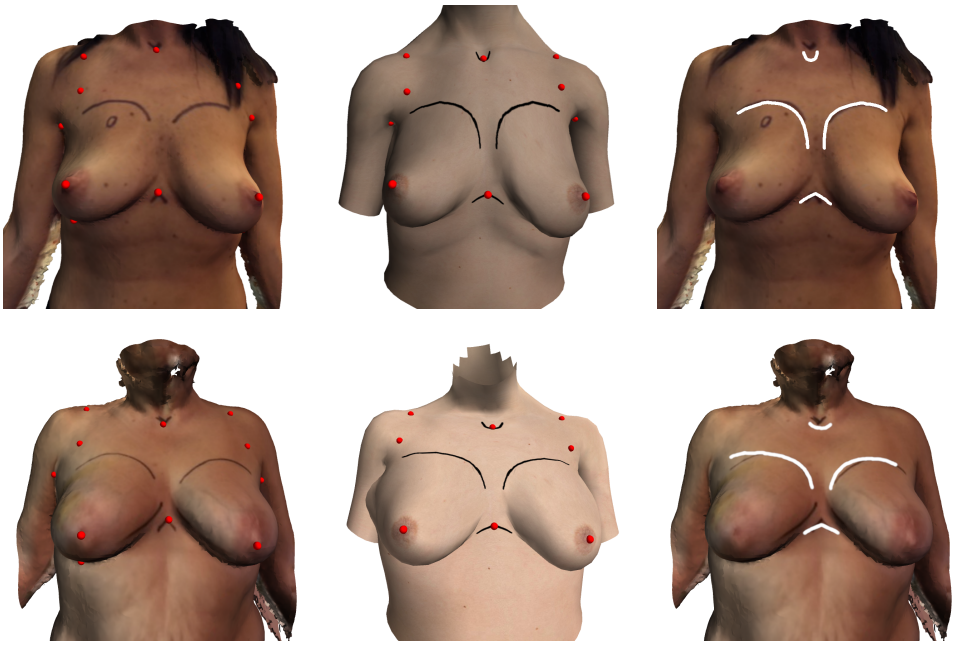

(a) Scan of patients 1 and 6 in preoperative stance

(b) Model registered on the preoperative patient scan

(c) Superimposition of the scan pattern (black) and model pattern (white)

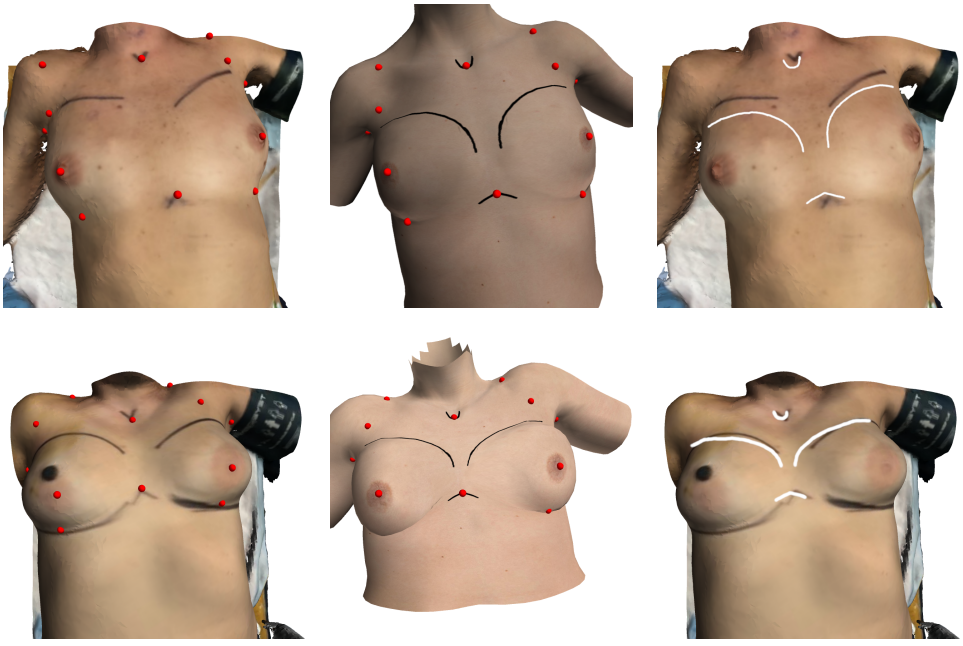

(d) Scan of patients 1 and 6 in intra-operative stance

(e) Model registered on the intra-operative patient scan

(f) Superimposition of the scan pattern (black) and model pattern (white)

Figure 9

References

[1] Ilya Baran and Jovan Popovi. Automatic rigging and animation of 3D characters. *ACM Transactions on Graphics*, 26(3), 2007. doi:10.1145/1275808.1276467.

[2] Paul J Besl and Neil D Mckay. A Method for Registration of 3-D Shapes. *IEEE Transactions on Pattern Analysis and Machine Intelligence*, 14(2):239–256, 1992. doi:10.1109/34.121791.

[3] S Bessa, Pedro H Carvalho, and P Oliveira. Registration of Breast MRI and 3D Scan Data Based on Surface Matching. *In Proceedings of the IEEE 16th International Symposium on Biomedical Imaging*, 2019. doi:10.1109/ISBI.2019.8759306.

[4] Sílvia Bessa, Pedro F Gouveia, Pedro H Carvalho, Cátia Rodrigues, Nuno L Silva, Fátima Cardoso, Jaime S Cardoso, Hélder P Oliveira, and Maria João Cardoso. 3D digital breast cancer models with multimodal fusion algorithms. *The Breast*, 49:281–290, 2020. doi:10.1016/j.breast.2019.12.016.

[5] Huu Phuoc Bui, Satyendra Tomar, Hadrien Courtecuisse, Stéphane Cotin, and Stéphane Bordas. Real-time Error Control for Surgical Simulation. *IEEE Transactions on Biomedical Engineering*, 65(3):12, 2017. doi:10.1109/TBME.2017.2695587.

[6] Dan Casas and Miguel A Otaduy. Learning Nonlinear Soft-Tissue Dynamics for Interactive Avatars. *In Proceedings of the ACM on Computer Graphics and Interactive Techniques*, 2018. doi:10.1145/3203187.

[7] Michael P. Chae, Warren Matthew Rozen, Robert T. Spychal, and David J. Hunter-Smith. Breast volumetric analysis for aesthetic planning in breast reconstruction: A literature review of techniques. *Gland Surgery*, 5(2):212–226, 2016. doi:10.3978/j.issn.2227-684X.2015.10.03.

[8] Carol E DeSantis, Jiemin Ma, Mia M Gaudet, Kimberly D Miller, Ann Goding Sauer, Ahmedin Jemal, and Rebecca L Siegel. Breast Cancer Statistics , 2019. *American Cancer Society Journal*, 69(6):438–451, 2019. doi:10.3322/caac.21583.

[9] Björn Eiben, Vasileios Vavourakis, John H Hipwell, Sven Kabus, Cristian Lorenz, Thomas Buelow, Norman R Williams, M Keshtgar, and David J Hawkes. Surface driven biomechanical breast image registration. *In Proceedings of SPIE Medical Imaging*, 2016. doi:10.1117/12.2216728.

[10] Giovanni Maria Farinella, Gaetano Impoco, Giovanni Gallo, Salvatore Spoto, Giuseppe Catanuto, and Maurizio B Nava. Objective Outcome Evaluation of Breast Surgery. *In Proceedings of Medical Image Computing and Computer-Assisted Intervention – MICCAI 2006: 9th International Conference*, 2006. doi:10.1007/11866565_95.

[11] François Faure, Christian Duriez, Hervé Delingette, Jérémie Allard, Benjamin Gilles, Stéphanie Marchesseau, Hugo Talbot, Hadrien Courtecuisse, Guillaume Bousquet, Igor Peterlik, and Stéphane Cotin. SOFA: A Multi-Model Framework for Interactive Physical Simulation. *Soft Tissue Biomechanical Modeling for Computer Assisted Surgery*, 11:283–321, 2012. doi:10.1007/8415_2012_125.

[12] Nikolas Hesse, Sergi Pujades, Michael J Black, Michael Arens, Ulrich G Hofmann, and A Sebastian Schroeder. Learning and Tracking the 3D Body Shape of Freely Moving Infants from RGB-D sequences. *IEEE Transactions on Pattern Analysis and Machine Intelligence*, pages 1–12, 2019. doi:10.1109/TPAMI.2019.2917908.

[13] Alec Jacobson and Olga Sorkine. Stretchable and Twistable Bones for Skeletal Shape Deformation. *ACM Transactions on Graphics*, 30(6):1–8, 2011. doi:10.1145/2070781.2024199.

[14] Doug L James and Christopher D Twigg. Skinning Mesh Animations. *ACM Transactions on Graphics*, 1(212):399–407, 2005. doi:10.1145/1073204.1073206.

[15] Pushkar Joshi, Wen C Tien, Mathieu Desbrun, and Frédéric Pighin. Learning controls for blend shape based realistic facial animation. *In Proceedings of 2003 ACM SIGGRAPH/Eurographics Symposium on Computer Animation*, 2003. doi:10.1145/1198555.1198588.

[16] Ladislav Kavan, Steven Collins, Jiří Žára, and Carol O'Sullivan. Geometric skinning with approximate dual quaternion blending. *ACM Transactions on Graphics*, 27(4):1–23, 2008. doi:10.1145/1409625.1409627.

[17] Youngjun Kim, Kunwoo Lee, and Wontae Kim. 3D virtual simulator for breast plastic surgery. *Computer Animation and Virtual Worlds*, pages 33–47, 2008. doi:10.1002/cav.237.

[18] R M Lacher, F Vasconcelos, N R Williams, G Rindermann, J Hipwell, D Hawkes, and D.Stoyanova. Nonrigid reconstruction of 3D breast surfaces with a low-cost RGBD camera for surgical planning and aesthetic evaluation. *Medical Image Analysis*, 53:11–25, 2019. doi:10.1016/j.media.2019.01.003.

[19] René M Lacher, Francisco Vasconcelos, David C Bishop, Norman R Williams, Mohammed Keshtgar, David J Hawkes, John H Hipwell, and Danail Stoyanov. A comparative study of breast surface reconstruction for aesthetic outcome assessment. *In Proceedings of Medical Image Computing and Computer-Assisted Intervention - MICCAI 2017: 20th International Conference,*, 2017. doi:10.1007/978-3-319-66185-8_58.

[20] Binh Huy Le and Zhigang Deng. Robust and accurate skeletal rigging from mesh sequences. *ACM Transactions on Graphics*, 33(4), 2014. doi:10.1145/2601097.2601161.

[21] J P Lewis, Ken Anjyo, Taehyun Rhee, Mengjie Zhang, Fred Pighin, and Zhigang Deng. Practice and Theory of Blendshape Facial Models. In *Proceedings of Eurographics 2014 - State of the Art Reports*, 2014. doi:10.2312/egst.20141042.

[22] Matthew Loper, Naureen Mahmood, Javier Romero, Gerard Pons-Moll, and Michael Black. SMPL : A Skinned Multi-Person Linear Model. *ACM Transactions on Graphics*, 34:248:1–248:16, 2015. doi:10.1145/2816795.2818013.

[23] Wan-Chun Ma, Yi-Hua Wang, Graham Fyffe, Bing-Yu Chen, and Paul Debevec. A blendshape model that incorporates physical interaction. *Computer Animation and Virtual Worlds*, 23:235–243, 2012. doi:10.1145/2073304.2073343.

[24] Chris Mills, Amy Loveridge, Alexandra Milligan, Debbie Risius, and Joanna Scurr. Is torso soft tissue motion really an artefact within breast biomechanics research? *Journal of Biomechanics*, 47(11):2606–2610, 2014. doi:10.1016/j.jbiomech.2014.05.023.

[25] Chris Mills, Amy Sanchez, and Joanna Scurr. Estimating the gravity induced three dimensional deformation of the breast. *Journal of Biomechanics*, 49(16):4134–4137, 2016. doi:10.1016/j.jbiomech.2016.10.012.

[26] Frederick I Parke. Computer generated animation of faces. *Proceedings of the ACM annual conference*, pages 451–457, 1972. doi:10.1145/800193.569955.

[27] Ganiyu A Rahman. Breast conserving therapy: A surgical technique where little can mean more. *Journal of Surgical Technique and Case Report*, 3(1):1–4, 2011. doi:10.4103/2006-8808.78459.

[28] H. Rappel, L. A.A. Beex, J. S. Hale, L. Noels, and S. P.A. Bordas. A Tutorial on Bayesian Inference to Identify Material Parameters in Solid Mechanics. *Archives of Computational Methods in Engineering*, 27(2):361–385, 2020. doi:10.1007/s11831-018-09311-x.

[29] Guillermo Ruiz, Eduard Ramon, Jaime García, Federico M Sukno, and Miguel A González. Weighted regularized statistical shape space projection for breast 3D model reconstruction. *Medical Image Analysis*, 47:164–179, 2018. doi:10.1016/j.media.2018.04.007.

[30] Maxime Tournier, Matthieu Nesme, Benjamin Gilles, and François Faure. Stable Constrained Dynamics. *ACM Transactions on Graphics, Association for Computing Machinery, in Proceedings of SIGGRAPH*, 34(4):132:1—-132:10, 2015. doi:10.1145/2766969.

[31] Chieh Han John Tzou, Nicole M Artner, Igor Pona, Alina Hold, Eva Placheta, Walter G Kropatsch, and Manfred Frey. Comparison of three-dimensional surface-imaging systems. *Journal of Plastic, Reconstructive and Aesthetic Surgery*, 67(4):489–497, 2014. doi:10.1016/j.bjps.2014.01.003.

[32] Rodolphe Vaillant, Loïc Barthe, Gaël Guennebaud, Marie Paule Cani, Damien Rohmer, Brian Wyvill, Olivier Gourmel, and Mathias Paulin. Implicit skinning: Real-time skin deformation with contact modeling. *ACM Transactions on Graphics*, 32(4), 2013. doi:10.1145/2461912.2461960.